Dynamic response of anchoring layered rock slopes subjected to seismic loads

Wei Zhou[1,2], Zhengman Ding[3,4] and Tingting Ma[3,5,6,*]

[1]College of Civil Engineering, Hunan City University, Yiyang 413000, China
[2]School of Civil Engineering and Architecture, Hubei University of Arts and Science, Xiangyang 441053, China
[3]College of Resource Environment and Tourism, Hubei University of Arts and Science, Xiangyang 440153, China
[4]Wufeng Tujia Autonomous County Forestry Bureau, Yichang 443099, China
[5]CAS Key Laboratory of Soil Environment and Pollution Remediation, Institute of Soil Science, Chinese Academy of Sciences, Nanjing 210008, China
[6]Hubei Key Laboratory of Low Dimensional Optoelectronic Materials and Devices, Hubei University of Arts and Science, Xiangyang 440153, China

The seismic dynamic responses of rock slopes are a hot topic for geotechnical engineering studies. Based on the interaction between rock slope and anchor bolts, a dynamic numerical model of a layered rock slope was developed using the finite difference software FLAC^{3D}. The dynamic response patterns of anchored and natural slopes under seismic loads were analysed to obtain the supporting effect of anchor bolts during seismic activity. The results indicate that under seismic loads, tensile cracks at the intersection of the top and joint surface develop into a drawing open surface of the back edge, and a shear slip occurs at the base of the slope, both of which result in the formation of tensile-shear slip failure. Permanent slope displacement accumulates only when seismic acceleration exceeds the critical acceleration. The slope deformation has been constrained, and the performance of the slope during the seismic activity has been strengthened by anchor bolt supports, which significantly increase the ductility of the rock slope under seismic loads. Moreover, during an earthquake, the axial forces of anchor bolts in the middle slope rise more than at any other position. After the earthquake, anchor bolts in the middle have been shown to exhibit maximum axial force. As a complex problem, stability analysis of seismic slopes is important. The analysis of seismic slope failure and the mechanism of slope anchoring are particularly complicated. The present study will help to improve future research on the seismic design and dynamic analysis of slopes supported by anchor bolts.

Keywords: Anchor bolts, anti-seismic effect, dynamic response, layered rock slope, seismic loads.

SEISMIC landslides are among the worst disasters in mountainous areas all over the world. As the main motivating factor, earthquakes could easily induce slope collapses, such as the 1995 Kobe earthquake in Japan[1] and the 2008 Wenchuan earthquake in China[2]. Seismic landslides have not only caused heavy casualties and substantial property damage[3] but have also induced physical dysfunction and post-traumatic stress disorder (PTSD) among the survivors and associated risk factors among children after the events, which poses a major threat to post-earthquake reconstruction[2,4,5]. Seismic stability of slopes and methods for enhancing seismic resistance of slopes under earthquake excitations are the most important engineering problems in geotechnical earthquake engineering. However, mitigation of the disasters posed by such events relies on whether we can fully predict the potential risk.

During the last decades, the problem of seismic landslides has been analysed by researchers using various methods, including field investigation[6,7], numerical simulation[8,9] and physical model tests[10–13]. In the practical application of solving slope stability problems, numerical simulations have more advantages in accuracy and affordability than field investigations and physical model tests. Griffiths and Lane[14] summed up the analysis results of slope stability on account of a shear-strength reduction technique, as well as described the merits and demerits of using the numerical method in practical applications of slope engineering. Wang *et al.*[15] carried out a general study on heavily jointed rock slope stability using Particle Flow Code 2 Dimensions (PFC2D) software. Choi and Chung[16] described the differences in two distinct constitutive models by simulating the stability of jointed rock slopes. Li *et al.*[17] analysed the influences of seismic parameters on the safety factor of bedding rock slopes under seismic load. Wang *et al.*[18] studied the dynamic response and axial stress distribution of rock bolts under explosive stress waves produced by concentrated charging. Xu *et al.*[19] analysed the dynamic response laws and the impact of ground motion parameters to the earthquake responses using the FLAC^{3D} program. Dong and Zhu[20] numerically examined the dynamic response of the slope supported with a framed anchor using the ADINA program. Li *et al.*[21] simulated the landslide process of Donghekou. Zheng *et al.*[22,23] numerically studied the failure of the fracture surface to slope due to an earthquake based on the FLCA dynamic strength reduction method. Taking into account the impact of mining activities, Xu *et al.*[24] numerically examined the landslide process of Jiweishan. A case study of Zhaoshuling landslide was carried out using FLAC^{3D} numerical simulation[25].

*For correspondence. (e-mail: ttmaxiaotu@126.com)

Table 1. Parameters of rock mass and joint used for simulation

Material	Density ρ (kg/m^3)	Elastic modulus E (GPa)	Poison ratio μ	Cohesive force C (kPa)	Internal friction angle φ (°)	Tensile strength σ_b (MPa)
Rock mass	2500	3.0	0.2	500	35	1.00
Joint	1700	0.01	0.3	120	20	0.05

Table 2. Physico-mechanical parameters of anchor bolts

Anchor length L (m)	Dip angle φ (°)	Separation distance s (m)	Elastic modulus E (GPa)	Poison ratio μ	Cross-sectional area A (mm^2)	Exposed perimeter p (mm)	Grout cohesive strength c_g (N/m)	Grout friction angle φ_g (°)	Grout stiffness k_g (N/m^2)	Normal cohesive force C_n (N/m)	Normal stiffness k_n (N/m^2)
32	15	2.5	200	0.25	314	189.6	1.75×10^5	30	1.0×10^9	1.75×10^8	1.0×10^9

Lv *et al.*[26] studied the dynamic response and failure mechanism of rock slopes during earthquakes. Chen and Wu[27] simulated landslide post-failure behaviour by two-dimensional discontinuous deformation analysis.

The finite difference method is among the most commonly used numerical analysis methods. FLAC^{3D} is a three-dimensional, explicit, finite-difference programme for engineering mechanics computation used extensively in geotechnical engineering[28–34].

In this study, a layered rock slope was established by FLAC^{3D} as the study object. The response patterns of unanchored and anchored slopes by earthquake loads were examined. The dynamic response pattern of axial forces of anchor bolts was also studied. The simulation results are expected to provide a theoretical basis and guidance for the seismic reinforcement design of the bedding rock slope.

Dynamic formulation

Model set-up

This study analyses a single-faced, homogenous rock slope studied by earlier researchers at 104 m altitude and incline angle of 75° (ref. 35) (Supplementary Figure 1 *a*). The selection of element size is mainly based on the frequency of the incident motion and the shear-wave velocity of the rock mass. In general, one-tenth of the shortest wavelength is chosen as the element size in the wave propagation direction[36]. This 0.1 m thick joint is simulated using a low-strength elastic–plastic element with a dip angle of 40°. The rock mass near the joint is considered a homogeneous body. Table 1 shows the basic parameters of the rock mass and joint in the simulation.

Supplementary Figure 1 *b* is a 2D sketch of the layout of the anchor bolts. Sixteen rows of anchor bolts were arranged in sequence (T01–T16) along the slope. Table 2 shows the basic parameters of anchor bolts used in the simulation.

As shown in Supplementary Figure 1 *c*, along the slope surface, the displacement monitoring sites numbered K01 to K10 are placed at an interval of 4.4 m from the peak of the slope to its foot. The displacement monitoring sites numbered P01 to P10 are placed at an interval of 2 m from the outside to the inside of the slope, and the length of each monitoring line is 52 m, parallel to the direction of the natural slope.

Boundary conditions and damping

Compared to static analysis, the reflected wave cannot dissipate when using fixed or elastic boundaries in dynamic analysis, resulting in simulation results with lower accuracy. An artificial boundary is introduced to reduce the impact of wave reflections in dynamic analysis. Free-field boundary is applied during the simulation process[37] (Supplementary Figure 2). Boundaries absorbed and attenuated the waves transmitting from inside out, with no obvious reflection back to the boundary.

Due to internal friction in materials, energy loss takes place when relative sliding occurs; this phenomenon is known as damping. An easy yet functional method for dynamic analysis is the so-called local damping, and its coefficient α_L is defined as

$$\alpha_L = \pi D,$$

where D is the critical damping fraction. Local damping of 0.0628 (i.e. the fraction of critical damping is 2%) was applied in the proposed model, following the suggestions of other researchers.

Earthquake loading

During the 2008 Wenchuan earthquake in China, a total of 1253 lines of main seismic accelerations were obtained. This is the largest and widest range of data recorded for mainland China so far and provides valuable seismic data for the study of dynamic problems under strong earthquakes[38]. The horizontal seismic acceleration wave applied in this study was obtained from the Wenchuan earthquake in

Shifang, Sichuan Province, China (Supplementary Figure 3). The peak value was 633.09 cm/s^2 at 37.41 s of the recorded seismic acceleration. To reduce the computation time and present better calculation results, a 35–50 s horizontal seismic acceleration time history was selected as the input seismic load.

Seismic records contain not only ground motion information during an earthquake but also complex noise. The low-frequency noise usually causes baseline drift, which often results in simulation inaccuracies. Thus, baseline correction is necessary. SeismoSignal software was used for baseline correction in this study, and Supplementary Figure 4 shows the results. It can be observed that the input earthquake loading for the total duration is 15 s (0.005 s as the time-step). The seismic load is transmitted from the bottom of the model to the top. The α_{max} value of the recorded earthquake is 1.633 g at 2.425 s. According to the acceleration time history, the velocity and displacement time histories can be obtained using one and two integrations respectively.

Results

Comparison of dynamic response patterns was made between the anchored slope and the natural slope under seismic loads. The dynamic calculation was done after the static balance.

Slope horizontal displacement response

Figure 1 shows the contour of the slope horizontal displacement after the earthquake. From Figure 1 *a*, an obvious slip between the slider and bedrock can be easily observed, with a peak horizontal displacement of 3.03 m at the intersection of the top and joint surface. This suggests that the slope has been destabilized under seismic load. Tensile cracks at the intersection of the top and joint surface develop into a drawing open surface of the back edge, and a shear-slip deformation occurs at the slope toe; both result in the formation of tensile–shear slip failure.

As shown in Figure 1 *b*, no obvious sign of slip can be found between the slider and bedrock. There is a maximum horizontal displacement of 0.168 m at the intersection of the top and joint surface. Compared with the peak horizontal displacement of the natural slope, the value decreases by 94.5%, indicating that anchorage support can significantly enhance the anti-sliding and anti-deformation ability of a slope under seismic load.

Supplementary Figure 5 shows the displacement recorded in the horizontal direction at the peak of the slope, together with the acceleration of the seismic wave during the earthquake. It can be observed that point K01, one of the arranged displacement monitoring sites in the horizontal direction, increases slightly in the first 7 s. However, it suddenly increases sharply when the seismic action time is 7 s. At the end of the earthquake action time, the final horizontal displacement of K01 is 2.238 m. This phenomenon indicates that a tension failure has occurred at the top of the slope when the earthquake acts for 7 s, and a slip failure has appeared from 7 to 15 s.

As seen in Supplementary Figure 5 *b*, a staged distribution curve can be obtained, which is the record of the horizontal displacement by time located at the summit of the model. In the first 6 s of seismic action time, it can be seen that the value increases slightly, which is the recorded monitoring displacement in a horizontal direction, and the value of the monitoring point displacement increases by 0.022 m. However, the displacement of K01 rises substantially from 6 to 9 s of the seismic, with a value of 0.104 m. From 9 s to the end, the K01 displacement tends to be stable, with a final value of 0.118 m. The results show that the permanent displacement of the anchored slope is not determined by the maximum acceleration but by the critical acceleration, which means that if the acceleration caused by the earthquake load cannot surpass the critical acceleration (e.g. 4–6 s), the displacement only fluctuates slightly, but the total displacement does not increase. Based on the Newmark method, 0.9 cm/s^2 is considered to be the critical acceleration, beyond which it is called relative acceleration. As shown in Supplementary Figure 5 *c* and *d*, the permanent displacement of a slope will appear only when the relative

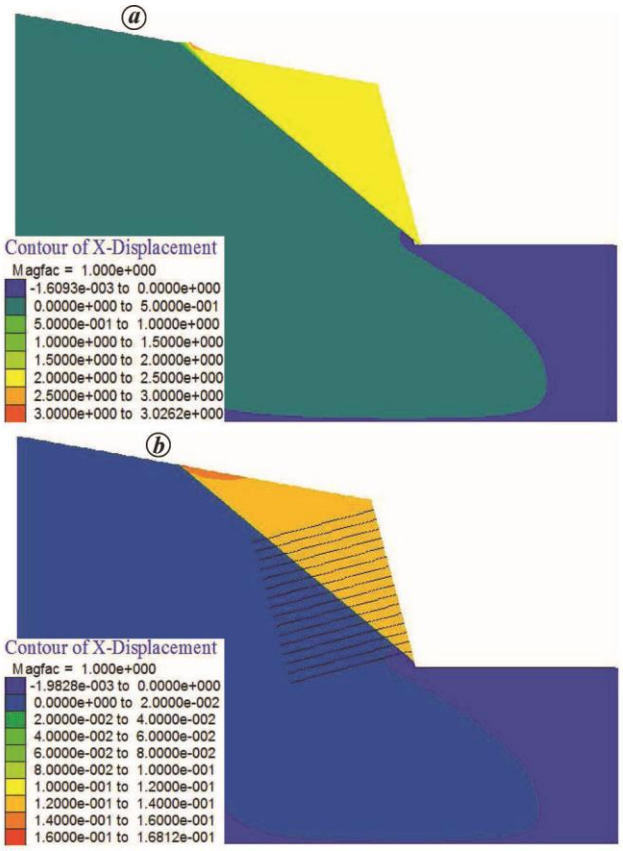

Figure 1. Contour of permanent horizontal displacement of (***a***) natural slope and (***b***) anchored slope.

acceleration is reached, proving the Newmark method's correctness. The maximum value of K01 is obtained after the acceleration caused by the earthquake reaches its peak, indicating that the ductility of the slope increase after anchorage (Supplementary Figure 5).

Supplementary Figure 6 presents typical variations in the horizontal displacement by time (P01–P10) towards the inclination of the slope. As seen in Supplementary Figure 6 *a*, the trends of monitoring horizontal displacements are almost identical in the direction of the natural slope. Along the anchor directly to the inside of the model, displacements in the horizontal direction of all monitoring points are reduced to zero after passing through the joint surface, indicating that the rock mass below the joint is stable. In addition, the relative displacement in the horizontal direction, which is located between the slide mass and rock mass, is approximately 2.235 m, indicating a distinct separation between the slide mass and rock mass. The displacement curve of P01 being slightly upwards might be because the area near P01 is close to the tension-slip displacement of the slopes.

As seen in Supplementary Figure 6 *b*, with the increasing height of the slope, the monitoring displacement in the horizontal direction increases; however, it reduces from the peak to the bottom of the model. The relative displacement between the slide mass and rock mass in the horizontal direction is about 0.113 m, suggesting the stable status of the anchored slope even under seismic loads.

Stress and strain response of the slope

Figures 2 and 3 present the contours of horizontal stress and shear stress of the slope respectively. As shown in Figure 2, the maximum stress in the horizontal direction of the natural slope and the anchored slope takes place at the intersection of the top and the joint surface separately, with values of 0.356 and 0.346 MPa.

In Figure 3, shear stress mainly occurs at the toe of the slope. The shear stress peak value is 0.46 MPa of the natural slope. For the anchored slope, the shear stress peak value is 0.59 MPa, indicating that the crest of the slope is easily damaged by tension stress and the foot of the slope is easily damaged by shear stress under seismic loads. This is in accordance with the results of Xu[39].

Figure 4 shows the contour of shear strain increments. The maximum shear strain increments of both slopes appear at the junction of the joint surface and the slope toe but decrease along the joint surface. The observed peak values of the shear strain increment are 5.1357 for the natural slope and 0.4575 for the anchored slope. This finding indicates that reinforcement of anchor bolts is beneficial for reducing shear strain increment of the slopes under seismic loads.

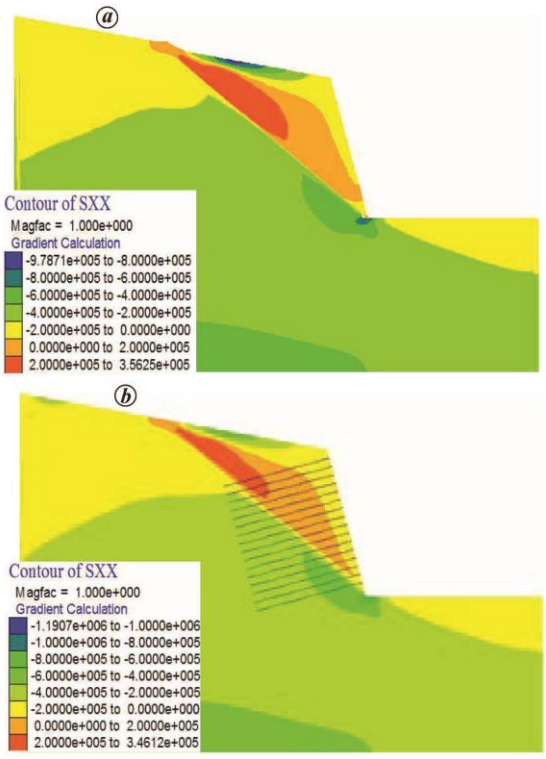

Figure 2 ***a***, ***b***. Contour of horizontal stresses of (***a***) natural slope and (***b***) anchored slope.

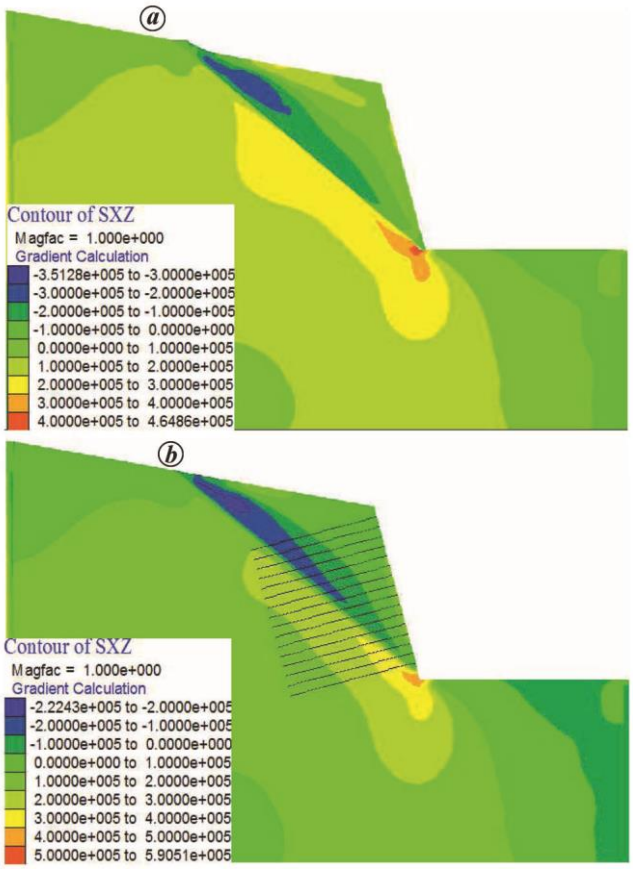

Figure 3 ***a***, ***b***. Contour of shear stresses of (***a***) natural slope and (***b***) anchored slope.

Dynamic response of anchor bolts

Supplementary Figure 7 shows the axial force distribution and displacement vector of anchor bolts after the complete dynamic event. Supplementary Figure 7 *a* reveals that the axial force distribution of anchor bolts is large in the middle but small at both ends. At the joint surface, the monitoring axial force reaches its peak, while it reaches its maximum at the joint surface. Supplementary Figure 7 *b* shows a downward sliding displacement along the slope surface of the anchor bolts in the slide mass. Anchor bolts in the rock mass remain stable, and no obvious displacement can be found. A comparison of Supplementary Figure 7 *a* and *b* reveals that the anchorage mechanism under seismic loads is because the slide mass has a downward sliding trend when the seismic loads act, the anchor bolts in the slope withstand axial tension, and the tension is gradually transmitted to the stable rock mass to keep the slide mass stationary. In this process, the anchor bolts play the role of 'shearing resistance and slide resistance' to limit the deformation of the slope.

According to the slope horizontal displacement response, tensile force occurs at the slope top under seismic loads. Therefore, the axial force of anchor bolt T01, selected as a typical monitoring bolt, was specified, and 32 monitoring points were set up along the anchor bolt per metre. Figure 5 shows the variations of axial force with time at these monitoring points during the earthquake. It can be observed that the axial force at the front and rear ends of anchor bolt T01 does not change significantly with earthquake action time. However, the axial force of T01 at the joint surface nearby increases with earthquake duration, especially the peak growth of the observed force at monitoring point no. 29, which is the closest to the joint surface. This is because slip deformation at the joint surface occurs as the earthquake load increases, resulting in an increase in the axial force of the anchor bolt. In addition, it can be observed that all the axial forces of the monitoring points increase in periodicity in the first 7 s, become stable at approximately 7 s, and then fluctuate around certain values until the end of the seismic action. This suggests that the deformation of the anchored slope becomes stable after 7 s of seismic action.

To study the axial force variation of the anchor bolt with time during an earthquake, rows 1 (slope crest), 8 (middle of the slope) and 15 (foot of the slope) of the anchor bolt elements at the joint surface were selected as typical monitoring points. Figure 6 shows the variation curve of the axial force with earthquake action time. It is observed that with the increase in the input time of seismic loads, the monitoring axial force also increases. The monitoring axial force at the top (T01) and foot (T15) of the slope increases from 113.12 to 530.56 kN and 243.92 to 472 kN at the first 7 s respectively. Thereafter, from 7 s to the end of the earthquake action time, the axial forces of T01 and T15 tend to be steady, finally fluctuating at constant values of 559.36 and 498.72 kN respectively. That is, the axial forces of T01 and T15 increase by 4.9 times and twice respectively, under seismic loads. There is a significant increment in the monitoring axial force located at the middle of the slope (T08), i.e. from 130.4 to 710.6 kN in the first 10 s. However, the pace of the increase of the axial force of T08 slows and a final value of 823.4 kN is obtained by the end of the shock. Thus the axial force of T08 increases approximately 6.3 times under seismic load.

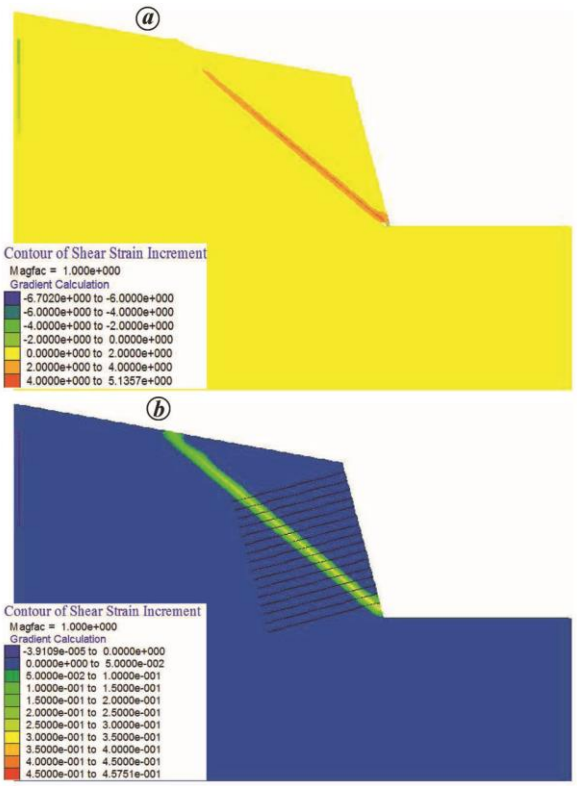

Figure 4 *a*, *b*. Contour of shear strain increments of (***a***) natural slope and (***b***) anchored slope.

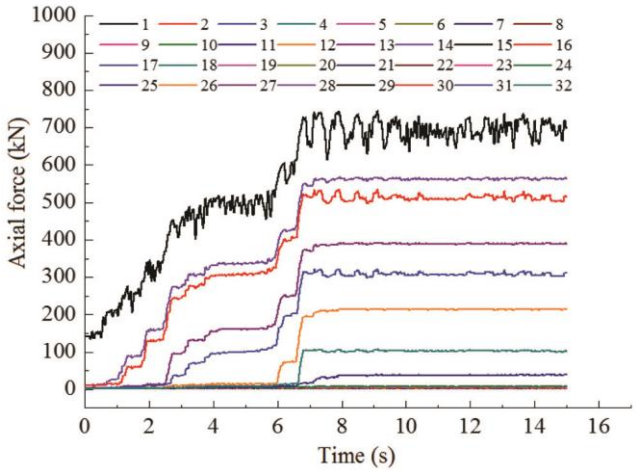

Figure 5. Axial force of anchor bolt T01. For the other annotations, refer to Figure 1.

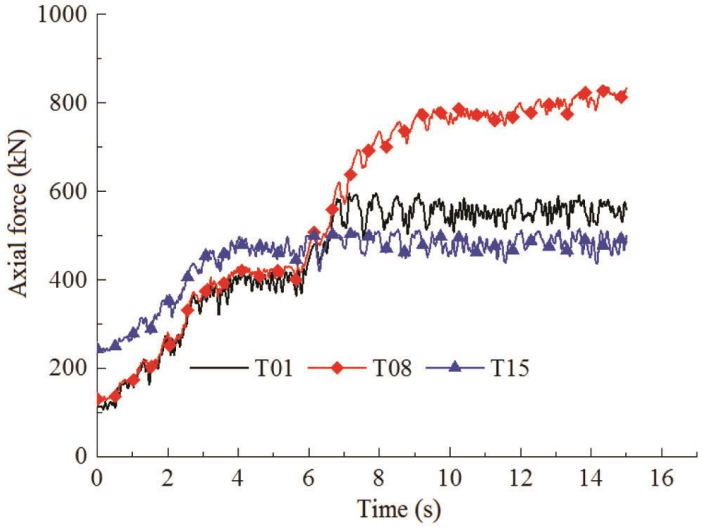

Figure 6. Axial force variation of selected anchor bolts at typical monitoring points of the joint surface from the crest (T01), middle (T08) and foot of the slope (T15) during an earthquake. For the other annotations, refer to Figure 1.

Supplementary Figure 8 shows the axial force variation of each anchor bolt located at the joint surface before and after the earthquake. The axial force of each anchor bolt is observed to increase significantly after the earthquake. The maximum enhancement of axial force in the anchor bolts occurs at the middle of the slope (T05–T12), with an approximately 6.74 times increase. The axial force of the anchor bolts located at the top (T01–T04) of the slope has a much smaller increase, with the minimum axial force increasing by 1.72 times; so does the axial force of anchor bolts located at the foot of the slope (T13–T16). Thus the axial force of the anchor bolts in middle increases more than any located at the top or foot of the slope during the earthquake. This result is consistent with the design concept of a 'strong waist and fixed foot' for the seismic code (GB 50011-2010).

Conclusion

There is progressive failure of the seismic slope as the earthquake proceeds. The deformation is caused by shear and tensile forces, eventually leading to instability and landslide failure. The failure zone formed by the shear force expands slowly from the foot upwards to the top, while the tension failure zone develops slowly from the top downwards to the foot, and finally achieves a cut-through between tension failure and shear failure zone. The permanent displacement of slope under seismic loads is determined by the critical acceleration. Only when the seismic acceleration exceeds the critical acceleration will bring permanent displacement of slope accumulate. Under seismic loads, a significant reduction in the slope deformation can be observed, and the aseismic performance of the slope enhances significantly after anchoring. Also, anchoring can increase the ductility of the slope as a whole. The axial force of the anchor bolts located in the middle increases that more than at the top or foot of the slope during the earthquake. At the end of the earthquake, the axial force of anchor located at the middle of the slope is the maximum, which indicates that the current design of anchor bolts supporting according to the average distribution of axial force per row is unreliable. The significant improvement in the axial force of the mid-slope anchor bolts must be seriously considered. As a complicated problem, stability analysis of the seismic slope, particularly slope failure under seismic loads and the anchoring mechanism, deserve further studies.

1. Hung, J. J., Chi-Chi earthquake induced landslides in Taiwan. *Earthq. Eng. Eng. Seismol*., 2000, **2**(2), 25–33.
2. Ni, J. *et al.*, Dysfunction and post-traumatic stress disorder in fracture victims 50 months after the Sichuan earthquake. *PLoS ONE*, 2013, **8**, e77535.
3. Park, S., Wooseok, Kim, W., Lee, J. and Baek, Y., Case study on slope stability changes caused by earthquakes – focusing on Gyeongju 5.8 ML EQ. *Sustainability*, 2018, **10**(10), 3441.
4. Lin, C. W., Liu, S. H., Lee, S. Y. and Liu, C. C., Impacts of the Chi-Chi earthquake on subsequent rainfall-induced landslides in Central Taiwan. *Eng. Geol.*, 2006, **86**(2), 87–101.
5. Zhang, S., Zhang, L. M. and Glade, T., Characteristics of earthquake- and rain-induced landslides near the epicenter of Wenchuan earthquake. *Eng. Geol*., 2014, **175**(11), 58–73.
6. Huang, R. and Li, W., Development and distribution of geohazards triggered by the 5.12 Wenchuan earthquake in China. *Sci. China Ser. E*, 2009, **52**(4), 810–819.
7. Aydan, Ö., Large rock slope failures induced by recent earthquakes. *Rock Mech. Rock Eng*., 2016, **49**(6), 2503–2524.
8. Abe, K., Nakamura, S., Nakamura, H. and Shiomi, K., Numerical study on dynamic behavior of slope models including weak layers from deformation to failure using material point method. *Soils Found*., 2017, **57**(2), 155–175.
9. Lv, Q., Liu, Y. R. and Yang, Q., Stability analysis of earthquake induced rock slope based on back analysis of shear strength parameters of rock mass. *Eng. Geol*., 2017, **228**(10), 39–49.

10. Wartman, J., Seed, R. B. and Bray, J. D., Shaking table modeling of seismically induced deformations in slopes. *J. Geotech. Geoenviron. Eng.*, 2005, **131**(5), 610–622.
11. Huang, R. Q., Zhao, J. J., Ju, N. P., Li, G., Min, L. L. and Li, Y. R., Analysis of an anti-dip landslide triggered by the 2008 Wenchuan earthquake in China. *Nat. Hazards*, 2013, **68**(2), 1021–1039.
12. Yu, J., Wang, R. B., Zhang, J. C., Yan, L., Meng, Q. X., Zhang, C. and Li, X. Z., Deformational characteristics of Donglinxin slope induced by reservoir fluctuation and rainfall. *Curr. Sci.*, 2017, **113**(6), 1159–1166.
13. Liu, X., He, C., Liu, S., Liu, Y., Lu, Y. and Liu, Z., Dynamic response and failure mode of slopes with horizontal soft and hard interbeddings under frequent microseisms. *Arab. J. Sci. Eng.*, 2018, **43**(10), 5397–5411.
14. Griffiths, D. V. and Lane, P. A., Slope stability analysis by finite elements. *Geotechnique*, 1999, **49**(3), 387–403.
15. Wang, C., Tannant, D. D. and Lilly, P. A., Numerical analysis of the stability of heavily jointed rock slopes using PFC2D. *Int. J. Rock Mech. Min. Sci.*, 2003, **40**(3), 415–424.
16. Choi, S. O. and Chung, S. K., Stability analysis of jointed rock slopes with the Barton-Bandis constitutive model in UDEC. *Int. J. Rock Mech. Min.*, 2014, **41**(S1), 581–586.
17. Li, H., Xiao, K. and Liu, Y., Factor of safety analysis of bedding rock slope under seismic load. *Chin. J. Rock Mech. Eng.*, 2007, **26**(12), 2385–2394.
18. Wang, G. Y., Zhang, S. H., Xie, W. Q. and Wan, X. D., Numerical analysis of dynamic response and axial stress distribution of rock bolts under explosive loads. *J. Min. Saf. Eng.*, 2009, **26**(1), 114–117.
19. Xu, G. X., Yao, L. K., Li, Z. H. and Gao, Z. N., Dynamic response of slopes under earthquakes and influence of ground motion parameters. *Chin. J. Geotech. Eng.*, 2008, **30**(6), 918–923.
20. Dong, J. H. and Zhu, Y. P., Analysis of response of slope supported with framed anchor to earthquake. *J. Lanzhou Univ. Technol.*, 2008, **34**(2), 118–122.
21. Li, X., He, S., Luo, Y. and Wu, Y., Simulation of the sliding process of Donghekou landslide triggered by the Wenchuan earthquake using a distinct element method. *Environ. Earth Sci.*, 2012, **65**(4), 1049–1054.
22. Zheng, Y. R., Ye, H. L. and Huang, R. Q., Analysis and discussion of failure mechanism and fracture surface of slope under earthquake. *Chin. J. Rock Mech. Eng.*, 2009, **28**(8), 1714–1723.
23. Zheng, Y. R., Ye, H. L., Huang, R. Q., Li, A. H. and Xu, J. B., Study on the seismic stability analysis of a slope. *J. Earthq. Eng. Eng. Vibrat.*, 2010, **30**(2), 173–180.
24. Xu, T., Xu, Q., Deng, M., Ma, T., Yang, T. and Tang, C. A., A numerical analysis of rock creep-induced slide: a case study from Jiweishan mountain, China. *Environ. Earth Sci.*, 2014, **72**(6), 2111–2128.
25. Li, D., Liu, X., Li, X. and Liu, Y., The impact of microearthquakes induced by reservoir water level rise on stability of rock slope. *Shock Vibr.*, 2016, **2**, 1–13.
26. Lv, Y., Li, H., Zhu, X. and Liu, W., Discrete element method simulation of random Voronoi grain-based models. *Cluster Comput.*, 2017, **20**(1), 335–345.
27. Chen, K. T. and Wu, J. H., Simulating the failure process of the Xinmo landslide using discontinuous deformation analysis. *Eng. Geol.*, 2018, **239**(18), 269–281.
28. Connell, L. D., Coupled flow and geomechanical processes during gas production from coal seams. *Int. J. Coal Geol.*, 2009, **79**(1), 18–28.
29. Ti, Z., Zhang, F., Pan, J., Ma, X. and Shang, Z., Permeability enhancement of deep hole pre-splitting blasting in the low permeability coal seam of the nanting coal mine. *PLoS ONE*, 2018, **13**(6), e0199835.
30. Ta, L. P., Matsumoto, T. and Hoang, H. N., Numerical studies on dynamic load testing of an open-ended pipe pile and a case study. *Geotech. Eng.*, 2014, **45**(2), 17–32.
31. Wang. M. M., Wang, G. L. and Wu, S. G., Stability analysis of soil behind a vertical free-face between supporting piles. *Eng. Geol.*, 2015, **195**, 155–163.
32. Li, Y., Jin, X., Feng, Y. and Luo, W., Effect of soft layer on seismic response of subway station in layered stratum. *J. Vibroeng.*, 2016, **18**(3), 1602–1616.
33. Lu, X., Song, M. and Wang, P., Numerical simulation of the composite foundation of cement soil mixing piles using FLAC^{3D}. *Cluster Comput.*, 2018, **1**, 1–10.
34. He, Z. M., Cai, Z. X., Cao, P., Liu, J. H. and Zhou, L. J., Numerical analysis for stratified rock slope stability reinforced by bolts. *J. Cent. South Univ.*, 2011, **42**(7), 2115–2119.
35. Kuhlemeyer, R. L. and Lysmer, J., Finite element method accuracy for wave propagation problems. *J. Soil Mech. Found. Div.*, 1973, **99**(5), 421–427.
36. St John, C. M. and Van Dillen, D. E., Rockbolts: a new numerical representation and its application in tunnel design. In Proceedings of the 24th US Symposium on Rock Mechanics, Texas A&M University, USA, 1983, pp. 13–24.
37. Cundall, P. A., Hansteen, H., Lacasse, S. and Selnes, P. B., NESSI – soil structure interaction program for dynamic and static problems, Norwegian Geotechnical Institute Report 51508-9, December 1980.
38. Tang, C., Ma, G., Chang, M., Li, W., Zhang, D., Jia, T. and Zhou, Z. Y., Landslides triggered by the 20 April 2013 Lushan earthquake, Sichuan Province, China: a case study in a region near the epicenter. *Eng. Geol.*, 2015, **187**, 45–55.
39. Xu, Q., Main types and characteristics of the geo-hazards triggered by the Wenchuan earthquake. *J. Geol. Hazards Environ. Preserv.*, 2009, **20**(2), 86–93.

ACKNOWLEDGEMENTS. This study was funded by the National Natural Science Foundation of China (42077143), Outstanding Young and Middle-aged Science and Technology Innovation Team Project of the Hubei Provincial Department of Education (HPDE) (T2020016), and the Training Fund Programme for Scientific Research of Hubei University of Arts and Science (2019 KYPY001 and 2020KYPYTD005), China.

Received 4 August 2021; revised accepted 6 November 2022

doi: 10.18520/cs/v124/i9/1088-1094